

# Turbulent channel flow with spatially-dependent viscosity: a numerical study

**Victor Coppo Leite\***

Research Assistant, Student Member of ASME

Ken and Mary Alice Lindquist Department of Nuclear Engineering  
Pennsylvania State University  
University Park, Pennsylvania 16802  
Email: vbc5085@psu.edu

**Elia Merzari**

Associate Professor, Member of ASME

Ken and Mary Alice Lindquist Department of Nuclear Engineering  
Pennsylvania State University  
University Park, Pennsylvania 16802

## ABSTRACT

*In the present study, we examine in detail the effect of spatially dependent viscosity on wall-bounded flow. For this purpose, Direct Numerical Simulations (DNS) are performed considering a channel flow with a viscosity change along the streamwise direction. The DNS were performed using Nek5000, a computational fluid dynamic (CFD) code developed at Argonne National Laboratory (ANL). The channel is divided in three different regions: in the first one, the flow is at a constant Reynolds number of  $Re = 5,000$ ; in the second region, the Reynolds number is imposed to linearly increase as viscosity decreases through a ramp of length  $L_{ramp}$ ; finally, in the third region the flow is again at a constant Reynolds number, this time at  $Re = 10,000$ . Since the temperature field is not evaluated, the proposed set up is a simplification of a heated channel. Nevertheless, the*

---

\*Address all correspondence to this author.

*outcomes of this study may be valuable for future works considering variable-viscosity effects, especially for cooling and heating applications. Four test cases with different ramp inclinations were analyzed. The set up is reminiscent of a transient channel flow, but with a space-dependent viscosity rather than a time dependent viscosity. The local results from the present study were compared with a correlation available in the literature for the friction Reynolds number as a function of the Reynolds number. We observe that in all cases the ramp does not cause an immediate change in the characteristics of turbulent structures in the second region and a delay is in fact observed in both wall shear and friction. Additionally, for shorter ramps we clearly see a burst in the turbulence field at the beginning of the third region. Finally, in order to characterize and understand these effects, low-speed streaks from the viscous region and turbulence statistics for the turbulent kinetic energy (TKE) budget terms are analyzed.*

## NOMENCLATURE

- $a$  Viscosity linear coefficient.
- $C$  Contraction parameter.
- $P$  Bump width parameter.
- $R$  Relaxation parameter.
- $Re$  Reynolds number.
- $Re_\tau$  Friction Reynolds number.
- $Re_\tau^*$  Delayed Friction Reynolds number.
- $u_\tau$  Friction velocity.
- $x$  Streamwise direction.
- $y$  Wall-normal direction.
- $z$  Spanwise direction.
- $\delta$  Half-height of the turbulence channel.
- $\delta_i$  Streamwise position where Region  $i$  starts,  $i=I, II$  and III.
- $\Lambda$  Signal contribution in the delayed function.

$L_{ramp}$  Ramp or Region II size

$W$  Low speed streak's width.

$\nu$  Kinematic Viscosity.

$\tau_w$  Wall Shear stress

## INTRODUCTION

Heat exchangers, combustion chambers and nuclear reactors are typical examples of engineering applications where turbulent flows feature strong temperature gradients, thus spatial distribution of thermal or viscous properties are relevant for their design. Heat removal is often carried out by single-phase flows in nuclear reactors. Particularly in test reactors, we observe sharp changes in molecular viscosity whereas density presents limited changes. For example, considering an average temperature increase of 40 K across the core of a test reactor operating with water at atmospheric pressure, the viscosity can drop to half of its original value, while density changes only by 2%. This fashion, the Reynolds number increases on the order of two-folds across the channel, meaning that turbulence undertakes significant changes throughout the length. Besides the engineering applications, the study of spatially dependent properties may also improve our understanding on turbulence phenomenon. The present study aims investigate the effect of spatially varying viscosity in a turbulent flow field. For that, we have extended a turbulence channel in the streamwise direction and we impose the Reynolds number to linearly increase by varying the viscosity after a fixed position in that direction. Once the Reynolds reaches the upper value, viscosity is kept constant once again. We notice that the case is an approximation of the more realistic set up of a heated channel flow, aimed at separating the effect of streamwise and wall-normal viscosity gradients. Finally, we considered four different cases with different ramps lengths, thus four different ramp inclinations for the Reynolds number.

This test case was first proposed in an earlier study [1]. The primary findings from that paper showed that by increasing the Reynolds number across a channel flow by spatially varying the viscosity does not cause an immediate change in the size of turbulent structures and a delay is in fact observed in both wall shear and friction Reynolds number. In contrast to that work, we

consider for the present one new cases at lower Reynolds numbers, i.e. from  $Re = 5,000$  up to  $10,000$ , thus enabling a higher resolution.

We note that there is a severe lack of data in the literature for flows undertaking this condition. In Refs. [2, 3], Zonta et al. performed numeric simulations to study variable-viscosity effects in forced convection flows. In these works, Zonta et al considered different Dirichlet boundary conditions on the walls' temperature of a turbulence channel yielding a temperature gradient in the vertical direction. Although they reported significant effects in that direction driven by viscosity spatial variations, they were not able to identify any effect in other directions as the flow is homogeneous in both streamwise and spanwise directions. That is, their case is different from ours once the Reynolds' ramp region causes the flow to become non-homogenous also in the streamwise direction.

As a matter of fact, results from the present work are reminiscent to an imposed excursion flow rate, but here the response in the turbulence field has a spatial dependence rather than a time dependence. In Ref. [4], it was shown that the transient flow for a channel experiencing an increase from  $Re = 2800$  to  $Re = 7400$  features a laminar-turbulent bypass transition even though the initial flow is turbulent. In this work He and Seddighi shows that after a rapid flow rate excursion a new boundary layer featured by a high strain rate is formed near the wall. Counterintuitively, this condition does not progressively evolve to a new turbulence field. Instead, following to the excursion it presents itself termed by these authors as laminar-like or pseudo-turbulent flow. In this situation, the pre-existing turbulent structures act as initial perturbations to the new flow field much like the role that the free-stream turbulence (FST) plays in a boundary bypass transition as proposed in Ref. [5]. The former turbulent structures are modeled into elongated streaks, which are structures often first formed in transition flows, Ref. [6]. Anyway, the case here considered does not undertake a bypass such as in Ref. [4], however it features different delays presents not only in that study but also in other studies related to rapid transients, here we mention Refs. [7–10]. The authors found that in a flow with a rapidly increasing Reynolds number, turbulence is initially frozen everywhere, and then it starts to increase first in the near wall region propagating towards other regions.

In addition to this discussion, former studies [11–14] has demonstrated that for accelerating flows, turbulence is generally attenuated while it is enhanced where the flow decelerates. Furthermore, other studies [15–17] have also investigated the effect of spatially accelerating and decelerating the flow throughout streamwise curvatures. We note however the difference in causation of such delays and local partial re-laminarization compared to the present case.

In the present work the flow is not being accelerated, and the Reynolds number is not changing due to a rapid excursion in time. The primary driver is a reduction of the viscous forces as viscosity changes in space. To investigate this effect Direct Numerical Simulations (DNS) are performed. These simulations were developed using Nek5000, a spectral-element code developed at Argonne National Laboratory (ANL) [18]. Our goal in this paper is to shed further light on the flow physics involved in this case. A secondary goal is to generate data for the assessment of Reynolds Averaged Navier-Stokes models.

Four effects have been identified and they are all related to different delays in the turbulence field. Firstly, turbulence does not respond immediately as the Reynolds number increases in space. We have developed a convolution analysis in the third section of the present article that aims modeling a spatial delay in a friction Reynolds number computed by a correlation valid for fully developed flows. This analysis showed that the flow does not behave as fully developed according to the imposed Reynolds number. Secondly, the peak of turbulence production shifts towards the core after the ramp region starts featuring a different energy distribution than the expected for fully developed flows. Additionally, the only budget term that does not feature this shift in the vertical direction accordingly to the production is the viscous diffusion. Thirdly, turbulence does not always evolve progressively along the ramp region as bursts takes place after this region depending on its inclination. These bursts were identified by a peak in the friction Reynolds number, peaks in the budget terms for the turbulent kinetic energy (TKE) and finally by the breakdown of streak structures in the near wall region. Finally, the fourth and last effect is related to the TKE redistribution after the ramp region, where once the turbulence bursts ceases it is noticed an energy redistribution in the normal direction as the budget terms converges to their expected values when far away from the ramp.

The work is structured as following: simulation details are provided in the second section, while the convolution function analysis mentioned above is presented in the third section. Next, the fourth section contains a discussion on the results: this includes the analysis of the delayed friction Reynolds number through the convolution analysis and how this delay is related to the budget terms of the TKE and the turbulent structures. Finally, the conclusion section provides a summary of the current findings and future works proposal.

## NUMERICAL METHODS AND MODEL DESCRIPTION

DNS of an incompressible Newtonian fluid with spatial-dependent viscosity is performed using Nek5000 [18] [19], an open-source code based on the spectral element method (SEM) introduced by Patera in Ref. [20]. In Nek5000 the domain is discretized by curvilinear hexahedral and quadrilateral elements and the solution is represented as a tensor-product of  $N^{th}$  order Lagrange polynomials built on  $N + 1$  Gauss Lobatto Legendre collocation points. For the present study, the  $P_N - P_{N-2}$  formulation for the pressure equation is employed. In this formulation the pressure field is solved at a lower polynomial order of the velocity field, in this case,  $N - 2$  order. Furthermore, Nek5000 features a stress-formulation solver capable of solving the three velocity components at once, this is essential for spatially dependent properties. Additionally, Nek5000 has received extensive validation in numerous references, we mention here Ref. [21, 22].

Figure 1 shows a sketch of the case set up considered. There are three regions in which viscosity is imposed differently: in Region I, viscosity remains constant and the flow is at a Reynolds number of  $Re = 5,000$ , in Region II viscosity decreases by the inverse of the streamwise length causing the Reynolds number to increase linearly from its former value up to  $Re = 10,000$ , and lastly in Region III, we impose viscosity to remain constant again but with a lower value. Worth's mentioning that in order to obtain a fully developed turbulent flow in Region I, a cyclic boundary condition has been considered for the first  $4\pi$  of that region.

For all cases we considered a channel with sizes of  $L_x = 20.0\pi$ ,  $\delta = 1.0$ ,  $L_z = 2.0\pi$ , where these parameters respectively represent: the streamwise length, the half-height and the spanwise length of the channel. Tab. 1 shows the flow conditions and mesh resolution of the four test

Table 1: Turbulence channel DNS details. Included details are: flow conditions, mesh resolution.

Case	$Re_I/Re_{III}$	$\Delta x^+$	$\Delta y_c^+$	$\Delta y_w^+$	$\Delta z^+$	$L_{ramp}$
I	5,000/10,000	10.5	13.7	0.3	0.7	$0.5\pi$
II	5,000/10,000	10.5	13.7	0.3	0.7	$1.0\pi$
III	5,000/10,000	10.5	13.7	0.3	0.7	$2.0\pi$
IV	5,000/10,000	10.5	13.7	0.3	0.7	$4.0\pi$

cases. In this table ,  $\Delta x^+$ ,  $\Delta y^+$  and  $\Delta z^+$  represents the grid spacing along the 3 directions and the superscript + indicates these values are in wall units, which is obtained upon normalization of the absolute grid spacing by the viscous lengthscale  $\delta_\nu = \nu/u_\tau$ , where  $\nu$  is the viscosity and  $u_\tau = \sqrt{\tau_w/\rho}$  is the friction velocity, being  $\tau_w$  the mean wall shear stress and  $\rho$  the density. We notice that for all cases, the finest lengthscales belongs to the third region, where the flow is at a higher Reynolds number. Additionally, Figs. 2 shows how viscosity and the corresponding Reynolds number is imposed to vary in the studied cases.

The domain is discretized with a grid of  $540 \times 16 \times 60$  elements with a non-uniform distribution in the vertical direction and a uniform distribution in both streamwise and spanwise directions. The total number of elements is 518,400 and Lagrangian polynomials up to the 11<sup>th</sup> degree have been employed. Finally, the mesh was designed to ensure enough resolution even in the harshest condition of the domain, for that, we referred to the mesh standards prescribed in Ref. [23] for

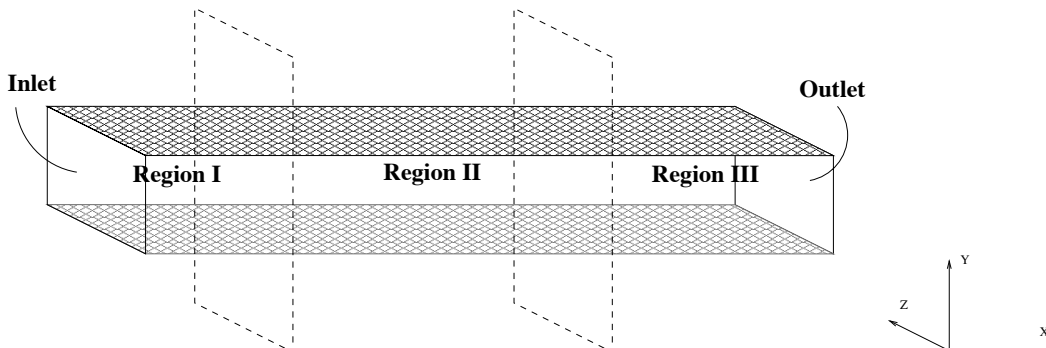


Fig. 1: Geometry of the turbulence channel, the channel is divided in three regions where viscosity is imposed to change.

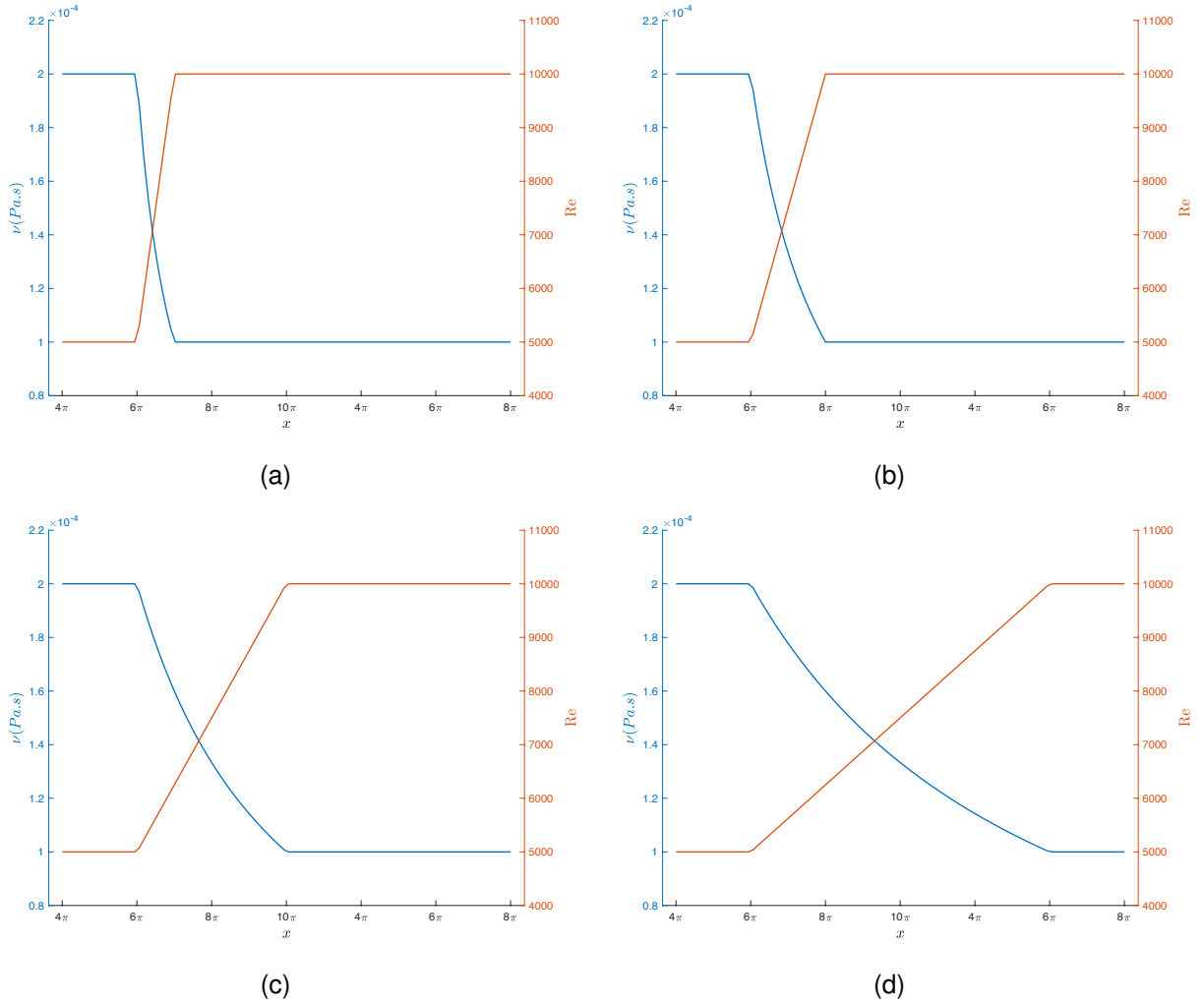


Fig. 2: Imposed  $\nu$  and corresponding  $Re$  throughout  $x$  for: (2a) Case I; (2b) Case II; (2c) Case III and; (2d) Case IV.

similar flow conditions that are being considered here. In that work, Lee et al. have performed DNS of incompressible channel flows up to  $Re = 125,000$ .

## CONVOLUTION ANALYSIS OF THE FRICTION REYNOLDS NUMBER

The friction Reynolds numbers calculated in the DNS from the present work were compared against the values of a correlation valid for fully developed flows from Ref. [24] through a convolution analysis. Eqn. 1 provides us with a correlation for the friction Reynolds number based on a given local Reynolds number considering that turbulence is fully developed. We notice that for our

cases, the Reynolds number is only a function of the viscosity, which depends only on  $x$ , meaning that the value yielded from Eqn 1 will also be only a function of  $x$ .

$$Re_\tau(x) = 0.09\{2Re(x)\}^{0.88} \quad (1)$$

As it will be shown in the results section, the friction coefficient reduces considerably in Region II due to the Reynolds ramp which induced a reduction in viscous forces. As observed in the introduction we expect that once Region II starts, the friction Reynolds number will not respond accordingly to Eqn. 1 if a sufficient spatial change into the flows condition is imposed. We expect that the DNS value will be delayed in space compared to the correlation value once turbulence is attenuated in this region.

We focus now on establishing a function depending on some parameters that will be used to modulate this delay. To derive this function we treat the friction Reynolds number from Eqn. 1 as a signal in space where a convolution operation is taken over it. The convolution operation is defined in Eqn 2. In this equation  $Re(\chi)$  stands for the analytical approximation provided by Eqn. 1,  $g(x - \chi)$  is a shifting function and  $\chi$  is simply a dummy variable for the streamwise distance.

$$Re_\tau^*(x) = \int_{-\infty}^{+\infty} Re_\tau(\chi)g(x - \chi)d\chi \quad (2)$$

The delaying function may be different throughout the three regions being considered, thus different shifting functions  $g(x - \chi)$  are employed depending on the region of interest. In the first region for instance, any delay should occurs, in this case  $g(x - \chi) = 1$  yields  $Re_\tau^*(x) = Re_\tau(x)$ , yielding the exactly behavior we are looking for.

Eqns. 3 and 4 shows the resulted convolution functions used in the present work to model the delay in Regions II and III respectively. For regions featuring delays, we employed functions

similar to exponential decays as shifting functions to obtain the convolution, following the approach suggested in Ref. [25].

$$Re_{\tau,II}^*(x) = \frac{a}{R^2}((x - \delta_{II})R + e^{-R(x-\delta_{II})} - 1) + 300 \quad (3)$$

$$Re_{\tau,III}^*(x) = 300(\sin\left(\frac{\pi}{P}(x - \sigma_{II})\right)e^{-C(x-\sigma_{II})} + \Lambda(1 - e^{-C(x-\sigma_{II})}) + Re_{\tau,II}^*(\sigma_{III})) \quad (4)$$

Where,

$Re_{\tau,i}^*(x)$  The delaying function for region  $i = II$  and  $III$

$\delta_i$  Location in  $x$  where Region  $i = II$  and  $III$  respectively starts

$R$  The relaxation parameter for Region  $II$

$P$  The bump width parameter for Region  $III$

$C$  The contraction parameter in Region  $III$

$\Lambda = 550 - Re_{\tau,II}^*(\delta_{II})$  A contribution in  $Re_{\tau}$  from Region II to III

The friction Reynolds numbers' values at a particular location do not depend only on the flow condition of that region, but also on values from upstream locations. In this context,  $R$  is referred as a relaxation parameter and it corresponds to the exponential decaying constant from the shifting function employed when deriving the convolution function for Region II. We note that this parameter allow us to delay the change in the friction Reynolds within the ramp region.

$P$  is the bump width parameter, which represents the burst of the friction Reynolds number right after the ramp region. Finally, we refer  $C$  as the contraction parameter, which corresponds to the exponential decaying constant employed in the shifting function to model the decay of the friction Reynolds number into its ultimate value, i.e. 550. Lastly, the values of these parameters for

the tested cases will be presented in the results section.

## RESULTS AND DISCUSSION

### Model Verification

In order to verify the model, results from first region were compared against existing data from Ref. [26] in which DNS results of a turbulent channel at  $Re_\tau = 300$  can be found. Fig. 3a shows the mean velocity  $\langle U \rangle^+$  versus  $y^+$  plot, while Fig. 3b shows the Reynolds stress  $\langle uu \rangle^+$ . The superscript indicates that non-dimensional values are plotted, here the normalization is done with  $u_\tau$  and  $u_\tau^2$  respectively. Figs. 3c and 3d shows the comparation with respectively the production  $P_k$  and the dissipation  $\epsilon_k$  terms from the TKE budgets for  $uu$ . In these two last terms, normalization is obtained with  $u_\tau^4/\nu$ . These graphs show us good agreement between the results and a relative error below 1.0% is found for any of the comparations. This way, these results grants confidence to the model developed.

### Flow Visualization

Fig. 4 provides a flow visualization of the streamwise velocity evolving in  $x$  for Case I as a reference case. By employing the appropriate scales in the gray color map, we are able to identify the large-scale features of the turbulent boundary layer. Furthermore, it becomes clear that these features appear to change in size after the ramp region, which is marked through a red square.

Next, Figs. 5 shows the development of the profiles of the average velocity  $\langle u \rangle$  and of the Reynolds stress component  $\langle u'u' \rangle$ , again for Case I as a reference. From Fig. 5a, we can clearly see that the viscous stress increases as viscosity decreases along the ramp region, i.e. from  $5.0\pi$  to  $5.5\pi$ . Due to that, we observe a redistribution in  $\langle u'u' \rangle$  component, which is shown in Fig. 5b and the thinning of the turbulent boundary layer, provided by the  $y^+ = 30$  curve in both plots.

### The Spatial Delay in $Re_\tau$

As observed, Eqns. 3 and 4, correspond to the delaying functions for Regions II and III respectively. In these functions, the  $Re_\tau(x)$  yielded by a correlation valid for fully developed flows is delayed in space. Furthermore, Region I does not have a similar function since no delay is

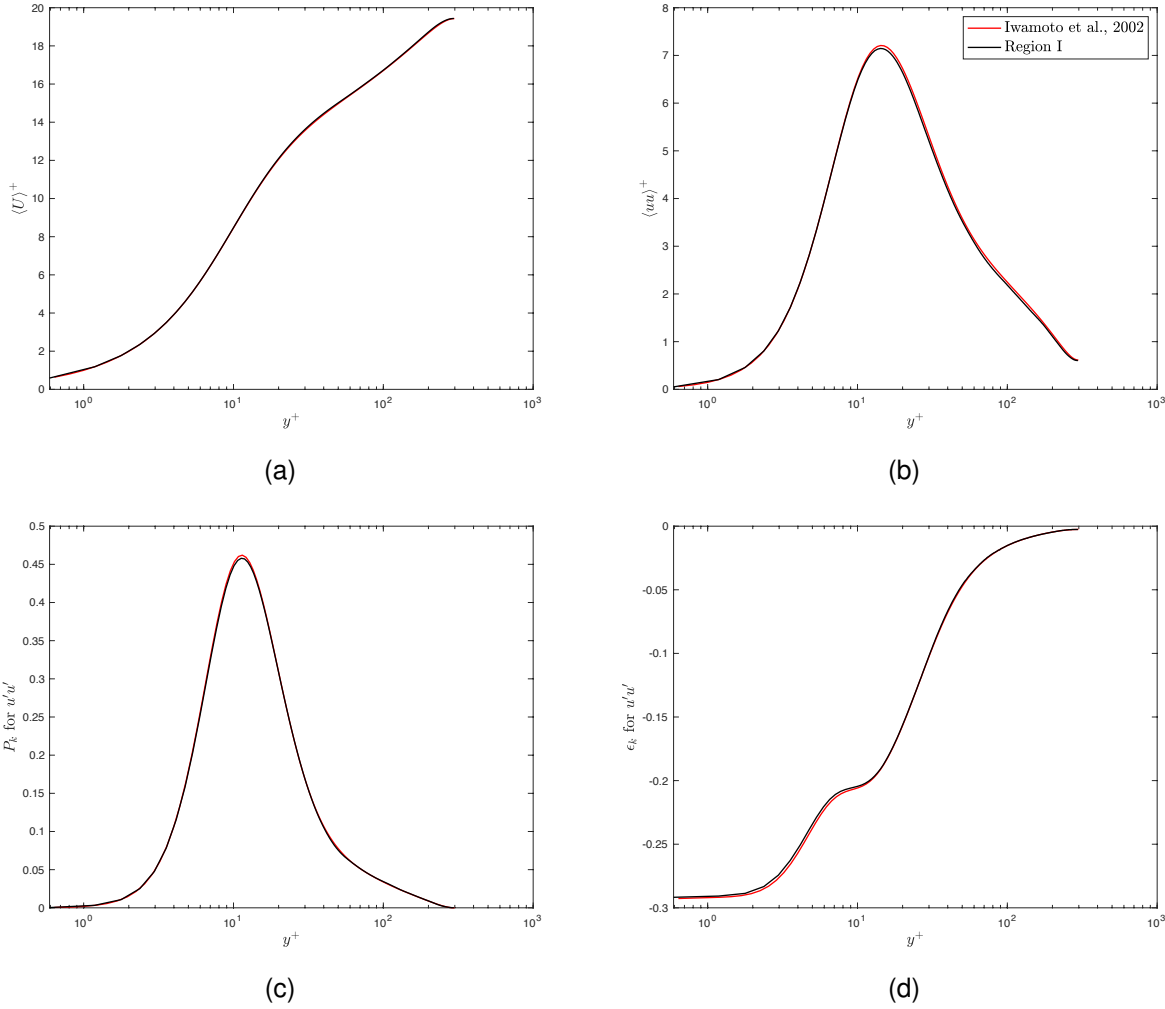


Fig. 3: Comparing statistics from Region I of our test cases and data from Ref. [26] at  $Re_\tau = 300$ . (3a) first order statistics,  $\langle U \rangle^+$  is compared. (3b) second order statistics,  $\langle uu \rangle^+$  is compared. (3c) the TKE production term  $P_k$  for  $uu$  is compared. (3d) the TKE dissipation term  $\epsilon_k$  for  $uu$  is compared.

expected for that region. In this approach, modeling the delay relies on the three parameters  $R_{II}$ ,  $R_{III}$  and  $C$ . Hence, our task becomes identifying these three parameters such that a good agreement between the delaying functions and the obtained data from the DNS is found.

Fig. 6 shows the result plots after exploring the parameter space for each parameter and identifying the best options for each of the cases defined in Tab. 1. It was possible to establish a good agreement between the friction Reynolds numbers calculated via DNS (red lines) and the values provided by the convolution functions that models the delay (blue lines) for the four tested

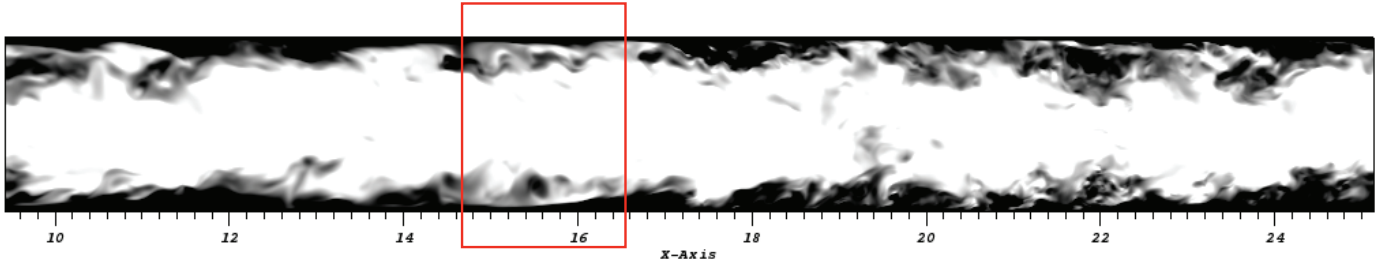


Fig. 4: Flow visualization of the streamwise velocity for Case I. The red rectangle marks the ramp region.

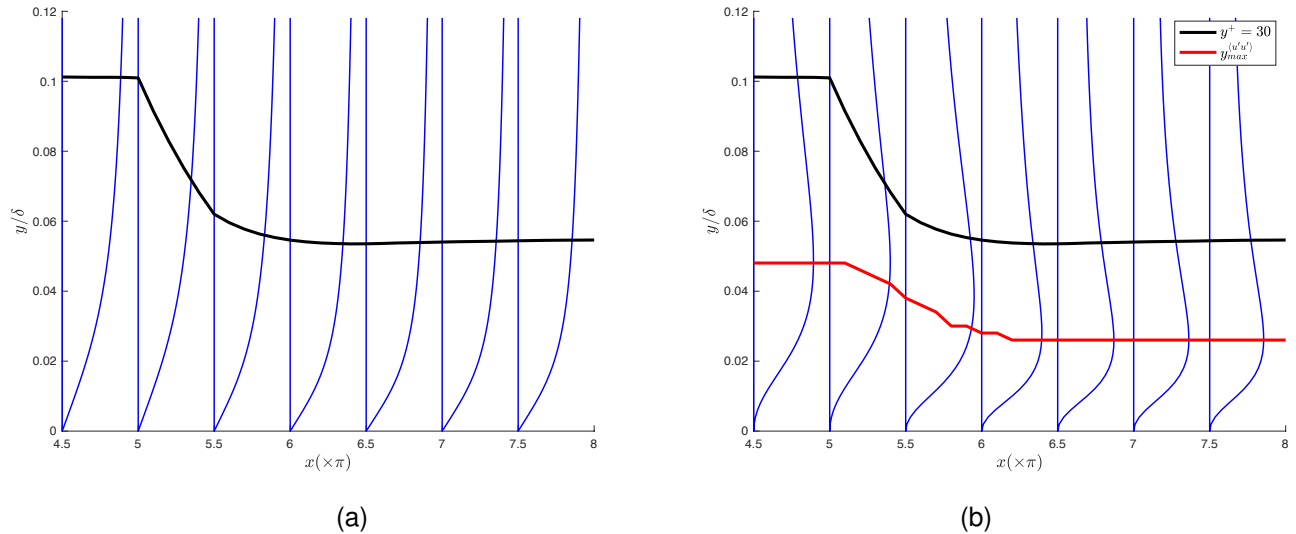


Fig. 5: The solid blue curves represent the development of: (a)  $\langle u \rangle$  and (b)  $\langle u'u' \rangle$  in the streamwise direction for Case I. In both plots the turbulent boundary layer at  $y^+ = 30$  is shown through a thick black line.

cases. In Cases I-III, a much clearer delay behavior for both Region II and Region III is found than for Case IV, where a larger ramp is considered. In all cases, during the ramp region, i.e. Region II, the value of friction Reynolds obtained via DNS does not increase as it would be expected if the flow were considered to be fully developed (black line). Additionally, it is clear that a bump in  $Re_\tau$  is formed right after Region II yielding a peak value in at the beginning of Region III. Specifically for Case III, we note that  $Re_\tau$  in Region II starts in a delayed regime and it reaches the corresponding value of the correlation provided by Eqn. 1 shortly before the end of the ramp region, roughly

Table 2: Delaying parameters values employed to obtain a good estimation for  $Re_\tau$  delay

Case	$L_{ramp}$	$x_{peak}$	$R$	$P$	$C$
I	$0.5\pi$	$6.3\pi$	$0.80 \pm 0.10$	$27.10 \pm 2.10$	$0.50 \pm 0.10$
II	$1.0\pi$	$6.6\pi$	$0.80 \pm 0.05$	$29.5 \pm 0.50$	$0.65 \pm 0.15$
III	$2.0\pi$	$7.4\pi$	$0.83 \pm 0.06$	$36.70 \pm 1.30$	$0.80 \pm 0.26$
IV	$4.0\pi$	$9.5\pi$	$0.86 \pm 0.06$	$\geq 120$	$0.85 \pm 0.45$

around  $x = 7\pi$ . Apparently for this case the flow has arrived at a fully developed condition at the end of Region II, however the presence of the bump in  $Re_\tau$  indicates that there is still some delayed effect taking place in the turbulence field that needs to be considered.

In Case IV we observe that the DNS  $Re_\tau$  is in much better agreement with the values from Eqn. 1 than the previous cases. Although the overall better agreement, we can see a small discrepancy in  $Re_\tau$  at the beginning of the ramp region. This discrepancy in Region II terminates roughly at  $x = 7\pi$ , where the corresponding  $Re_\tau$  from DNS and from Eqn. 1 becomes equal to each other. Thus, we can see that there might be a delay for Region II at least within the first  $2\pi$  of this region regardless the ramp inclination. Also, for Case IV, besides the abovementioned delay in Region II, we still can see a much less pronounced bump at the beginning of Region III when compared to Cases I-III.

To provide a more quantitative information about these effects, we refer to Tab. 2. This table presents the parameter values found after the tuning procedure that leads the convolution function to overlap the DNS results such that the root-mean-square deviation remains below 1.0% from DNS values. In this table  $x_{peak}$  stands for the streamwise position where the friction Reynolds reaches a maximum value. It is important to mention that although Region III is nearly flat for that Case IV,  $x_{peak}$  is still reported.

We observe that the ramp's length  $L_{ramp}$  enhances or prevents the effects in Region III (turbulence bursts) from taking place. Furthermore, we can identify different trends for the three delaying parameters:

$R$  This parameter largely remains constant with value  $R \approx 0.8$  regardless the length of the ramp

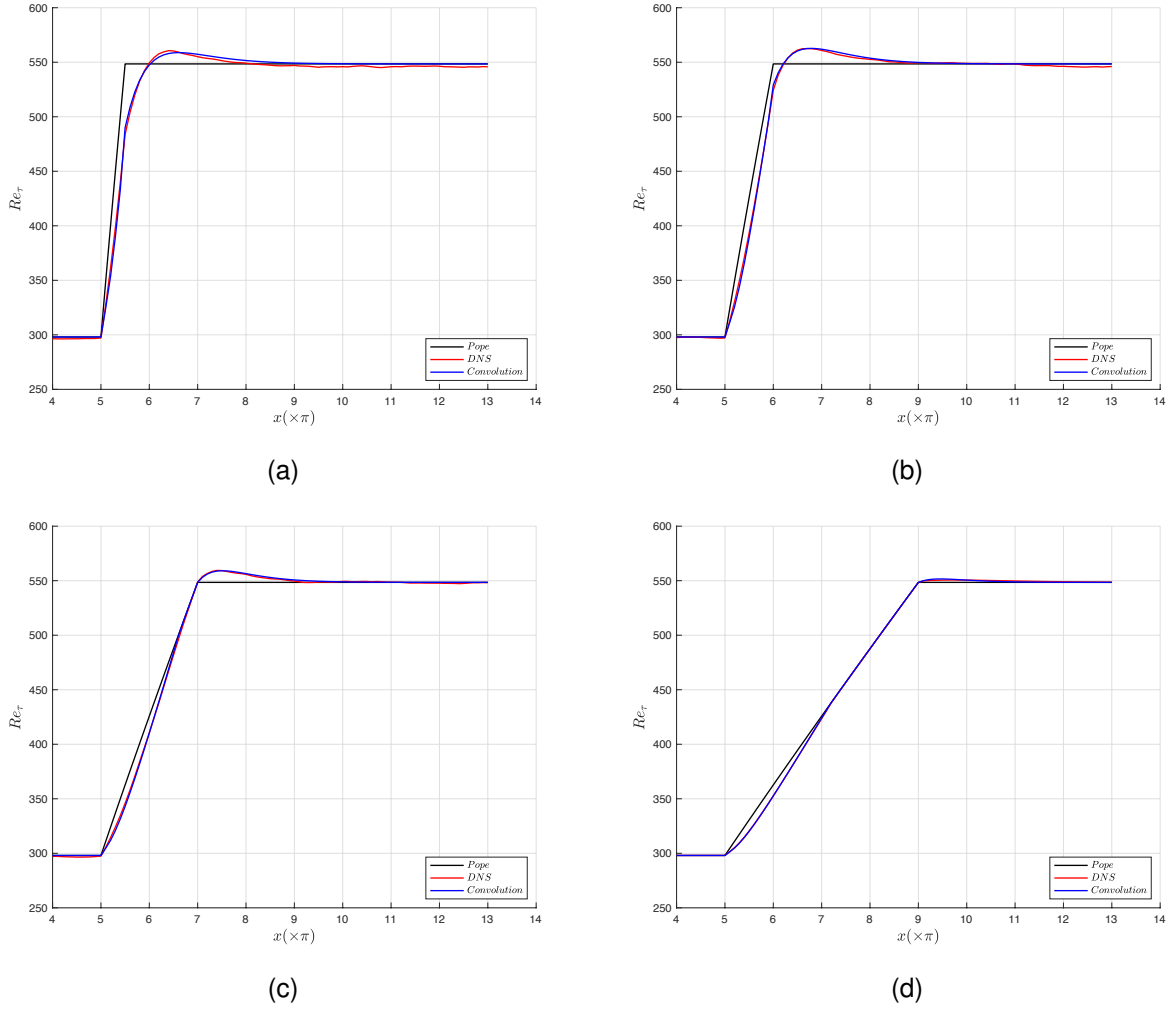


Fig. 6: Friction Reynolds number through  $x$  for: (6a) Case I; (6b) Case II; (6c) Case III and; (6d) Case IV (the convolution function is not shown for this case as it does not hold).

region  $L_{ramp}$ . In other words, the delay in Region II modeled by the convolution function is invariant to the ramp inclination imposed. This provides some evidence that the root cause of the delay effect in this region is actually shared among all test cases. We postulate that this delay is determined by the flow conditions at the outlet of Region I, i.e. fully-developed flow at  $Re_\tau = 300$ . Thus, the delay in the ramp region may not depend on other conditions, e.g. ramp inclination or ultimate flow condition. Actually, this feature is reminiscent of transient channel flow investigated in Refs. [4, 7–10]. In these works, instead of imposing a spatial change in the flow condition, a flow excursion is considered. Specifically, in Ref. [8], it is shown that

for several pipe transients there is no influence of the flow excursion rate on the delay in the response of the turbulence field.

- P* The bump width parameter modulates the overshooting of the friction Reynolds number in Region III. We notice that as the ramp region  $L_{ramp}$  increases, the bumps becomes less pronounced requiring greater values for this parameter. We notice that specifically in Case IV, where Region III is nearly flatten, this parameter can actually have any value as long as greater than a minimum threshold of 120.
- C* Similarly to the relaxation parameter  $R$ , we observe that the contraction parameter  $C$  largely remains constant throughout the four tested cases.

We note that in addition to the optimal values of the parameters Table 2 reports bounds of the parameters that give a maximum error of 2% compared to DNS data.

The convolution function proved to be a useful tool to evaluate some of the effects exhibited in the test cases. However, this effects still require a better characterization from the turbulence standpoint. In the following sections, we attempt to address that by investigating turbulence structures in the near wall region and turbulence statistics as well.

## **Turbulence Budgets**

Here we examine the influence of imposing varying viscosity on the TKE balance. For this purpose, we consider Eq. 5 that presents the TKE transport for an incompressible fluid with spatial dependent viscosity:

$$\frac{D \langle k \rangle}{Dt} = P_k + \Pi_k + T_k + D_k + \epsilon_k \quad (5)$$

Where,

$$\begin{aligned} P_k &= -\langle u'_i u'_j \rangle \frac{\partial \langle u_i \rangle}{\partial x_j} & \Pi_k &= -\frac{1}{\rho} \frac{\langle p' u'_i \rangle}{\partial x_i} & T_k &= -\frac{1}{2} \frac{\partial \langle u'_i u'_i u'_j \rangle}{\partial x_j} \\ D_k &= \frac{1}{2} \frac{\partial}{\partial x_j} \left[ \nu(x) \frac{\partial \langle u'_i u'_i \rangle}{\partial x_j} \right] & \text{and} & & \epsilon_k &= -\nu(x) \left\langle \frac{\partial u'_i}{\partial x_j} \frac{\partial u'_i}{\partial x_j} \right\rangle \end{aligned}$$

In the above equation the right-hand side term represents the material derivative of the TKE,  $\langle k \rangle \equiv \frac{1}{2} \langle u'_i u'_i \rangle$  and the right-hand side terms represents the budget terms for  $\langle k \rangle$ . Namely these terms represent:  $P_k$  the production,  $\Pi_k$  the pressure diffusion,  $T_k$  the turbulent diffusion,  $D_k$  the viscous diffusion and  $\epsilon_k$  the dissipation. The sum of these terms is zero for a statistically steady condition Ref. [24].

Figures 7-9 shows the distribution of the budget  $\langle u' u' \rangle$  terms along the vertical direction at different streamwise positions for Cases I-III respectively. Case IV is not reported for brevity as this case does not feature the characteristics from the discussion that follows. We note that these plots are normalized by  $u_\tau^4 / \nu$  with values from Region I so we can visualize absolute variations of these terms. For the analyzed cases, the TKE budget distribution along the vertical direction presents the usual features for fully developed flows at  $x = 5\pi$ , however it exhibits some differences in other regions. First, the maximum production location shifts towards the core deviating from the well-known position for this peak, which is around  $y^+ \approx 11$  Ref. [27]. In fact, this position shifts to  $y^+ \approx 14, 13$  and  $12$  in Cases I-III respectively. Although Case IV is not presented, it largely remains unchanged not featuring this kind of delay.

Second, right after the ramp region, the budget terms clearly overshoot their expected values for Region III. For example, curves specifically located at  $x_{peak}$  from Tab. 2 are provided in Figs 7-9. A potential explanation for that is provided in the next section in terms of the evolution of turbulence structures. In fact, we observe that the streaks coming from Region I does not start breaking down as soon as they enter in Region II, instead they only become unstable after a while. When they start breaking down and additional energy is then released. Furthermore, this additional turbulence is redistributed downstream. Lastly, we observe the only budget term that

does not shift in the vertical direction accordingly to the production peak is the viscous diffusion  $D_k$ .

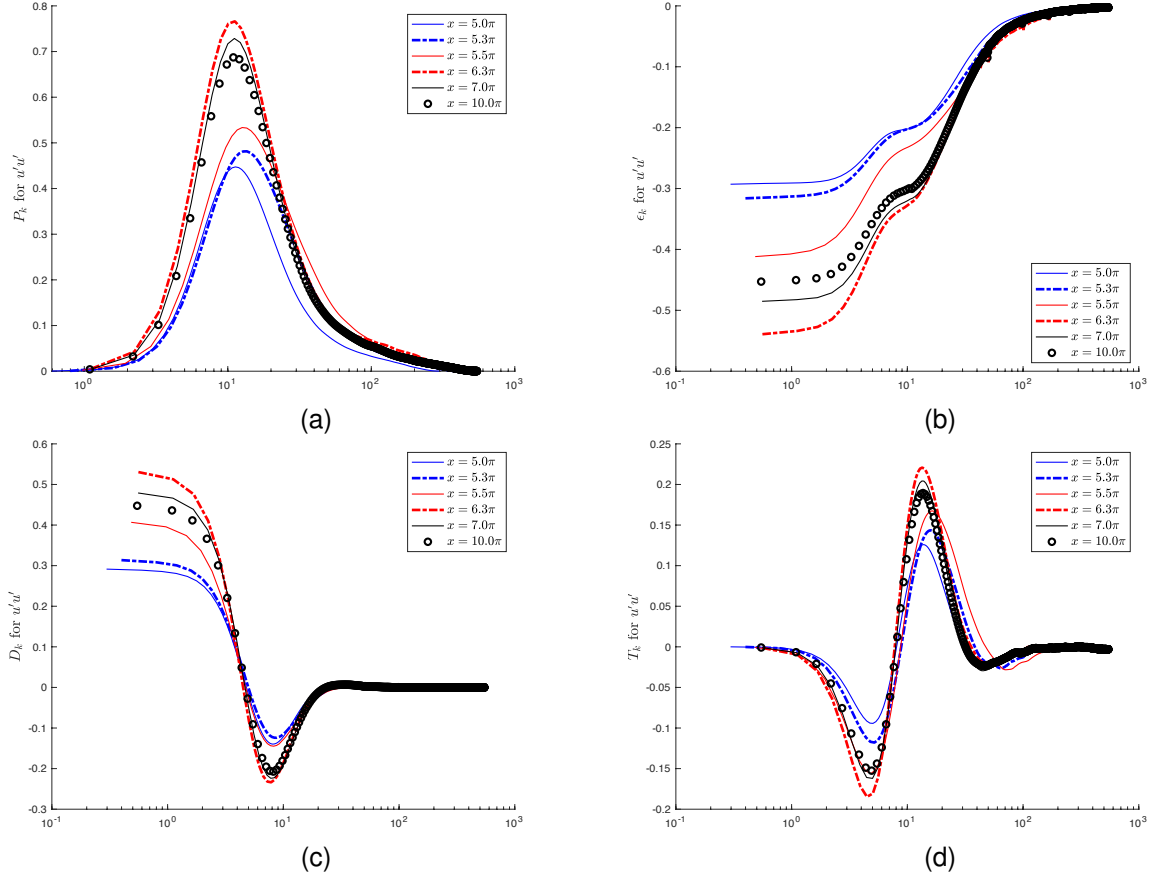


Fig. 7: The budget terms of  $\langle u'u' \rangle$  for Case I: (7a)  $P_k$  production; (7b)  $\epsilon_k$  dissipation; (7c)  $D_k$  viscous diffusion; (7d)  $T_k$  turbulent diffusion

## Turbulent Structures

The present section intends to explore the delays effects from the turbulence structures stand-point of view. Namely, we investigate low-speed streaks, Kline et al. in Ref. [11]. Figs. 10-13 shows the contours of the streamwise fluctuating velocity  $u$  from Cases I-IV respectively, the color map is provided over a plane parallel to the wall and placed at an absolute distance of  $y = 0.02$  from it. This distance was chosen to ensure that all structures being visualized belong to the viscous sublayer region once this plane corresponds to a non-dimensional distance of  $y^+ = 5.5$  in

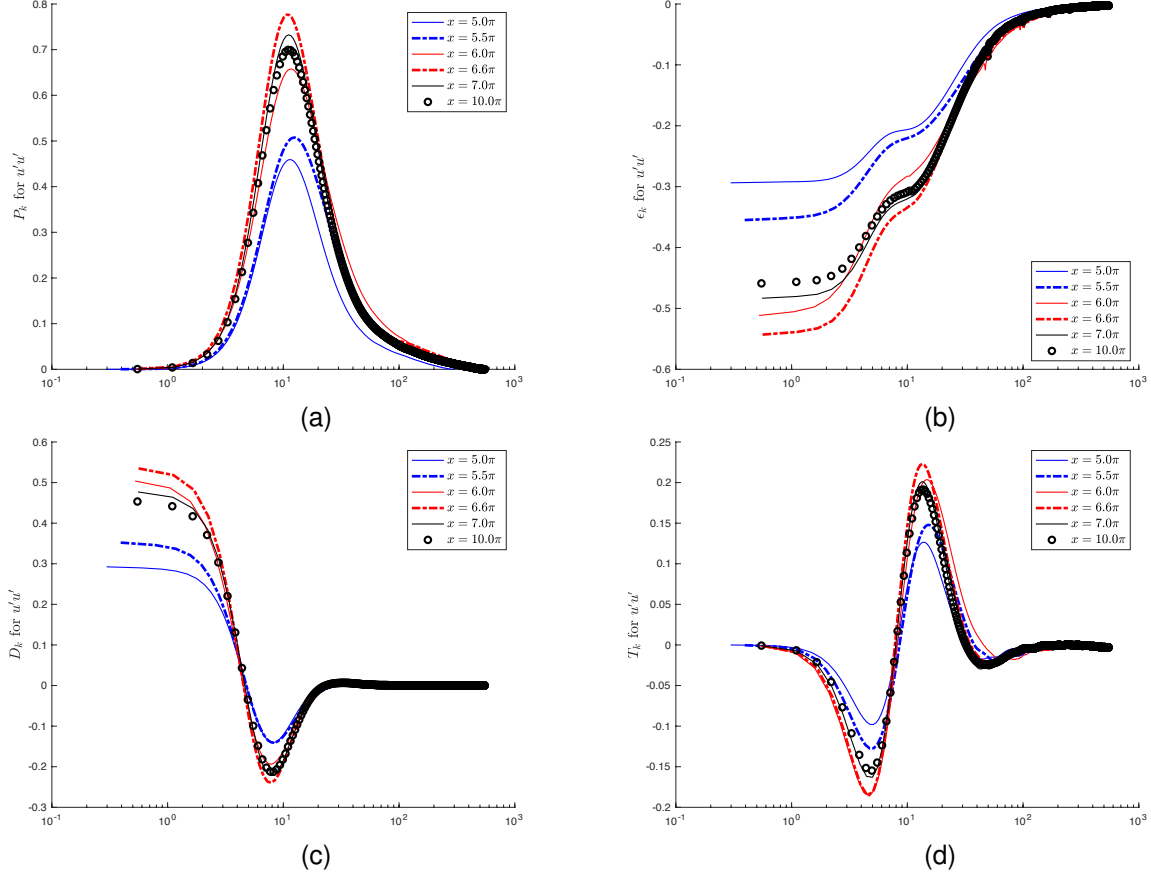


Fig. 8: The budget terms of  $\langle u' u' \rangle$  for Case II: (8a)  $P_k$  production; (8b)  $\epsilon_k$  dissipation; (8c)  $D_k$  viscous diffusion; (8d)  $T_k$  turbulent diffusion

wall units if we consider a normalization using the length scale of the third region. In the color maps red represents low speed structures ( $u \leq -30$ ) and blue color represent higher speed structures ( $u \geq 30$ ). Additionally, in order to help us investigate the flow response, Fig. 14 shows the computed friction coefficient  $C_f = \tau_w / (\rho U^2 / 2)$  throughout the streamwise direction for all cases.

In all cases from Figs. 10-13, the low-speed streaks remain stable for some period after the ramp region begins. Only after a given position they start breaking down into smaller structures. Specifically, for Cases I and II, these structures keep their streamwise length about the same size or sometimes even greater than the ramp's length itself. Differently, Cases III and IV have their ramp length  $L_{ramp}$  greater in value than Cases I and II and the breakdown of the streaks starts before the end of the ramp.

Regarding the friction coefficient, we note that this parameter reduces in value as a response

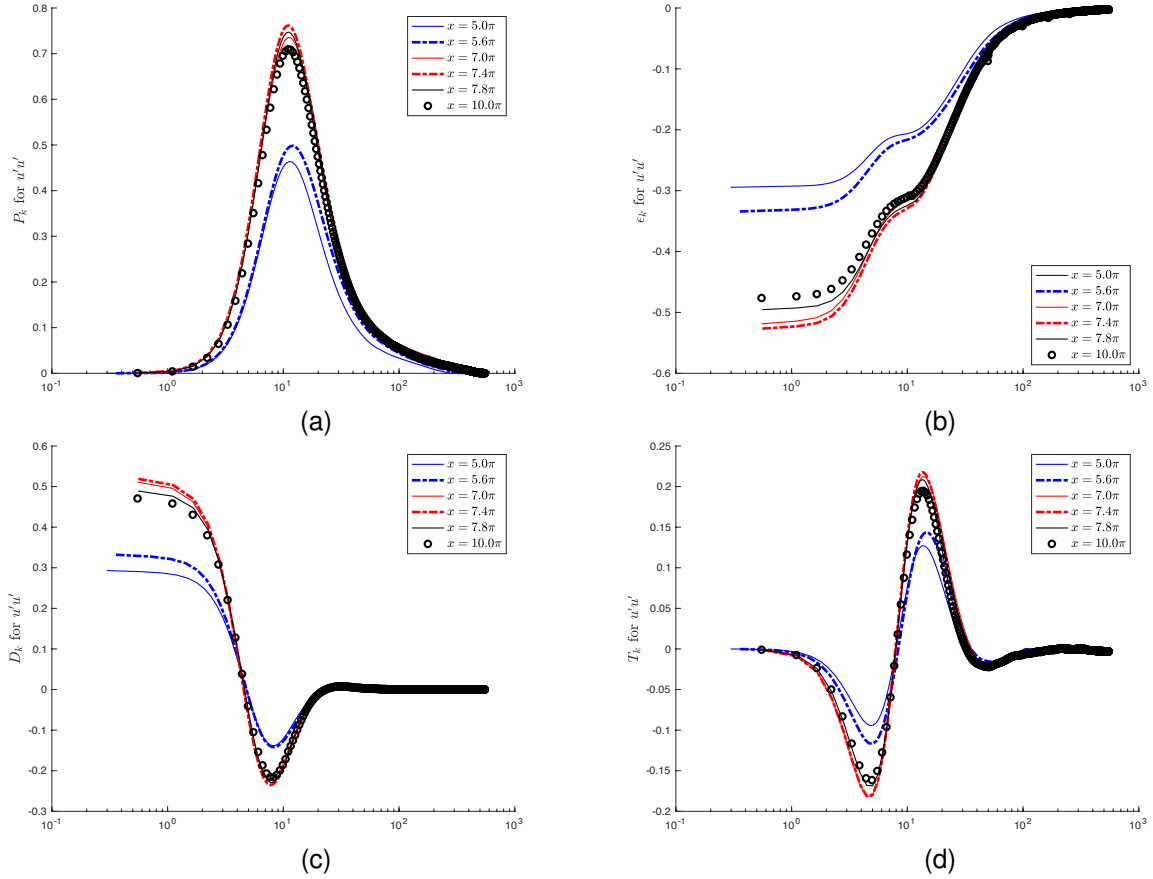


Fig. 9: The budget terms of  $\langle u'u' \rangle$  for Case II: (9a)  $P_k$  production; (9b)  $\epsilon_k$  dissipation; (9c)  $D_k$  viscous diffusion; (9d)  $T_k$  turbulent diffusion

to the ramp region regardless the case. For Cases I-III, which are featured by the convolution analysis,  $C_f$  further decreases reaching a minimum value within the ramp region. This scenario is remarkably similar to what is reported in the transient flows experiments from Refs. [4, 10] during the stage termed as pre-transition by the authors. Again, in Refs. [7–9] the authors found that in a rapidly accelerating flow, turbulence is initially frozen everywhere, and then it starts to increase first in the near wall region propagating towards other regions. In the present work the  $Re$  does not increase to a rapid excursion, but instead due to a decrease of viscosity as the flow goes through Region II. This scenario causes the streak structures keep their characteristics during the beginning of Region II.

As we shorten the ramp lengths  $L_{ramp}$  a much stronger reduction response in  $C_f$  is observed. Actually, throughout Region II from Case I,  $C_f$  behaves laminar-like as we find a good agreement

between the value yielded from the DNS and the Blasius solution [28]. Above that, we note that in general all four cases had turbulence attenuated within Region II. To show that, the Johnston's correlation  $C_f = 0.0706/Re^{0.25}$  valid for fully developed flows [29] is shown applied to Case IV.

By comparing the results from Fig. 14 with the corresponding cases in Figs. 10-13 we notice that  $C_f$  reaches a minimum value roughly at the same position where the streaks starts breaking down. Again, this is another striking similarity to the transient turbulent channel experiment once in Ref. [10], He and Seddighi observes the same kind of event, still though in their work they draw such comparison in time rather in space.

Finally, for Cases I-III, there is a clear discontinuous response for  $C_f$  at the end of the corresponding end of ramp featuring a sudden increases of this parameter. This abrupt response is followed by a peak in  $C_f$  in Region III. It is evident that these peaks are actually being caused by the turbulence bursts taking place after the ramp region. The  $x$  positions where these peaks

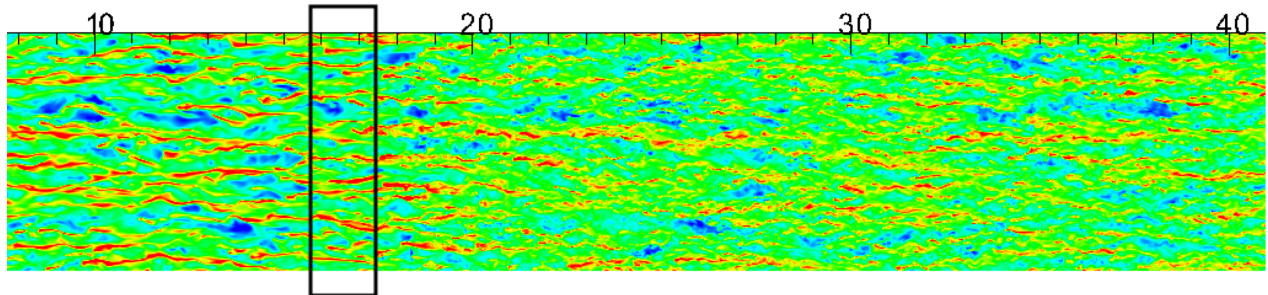


Fig. 10: Contour plots of  $u$  in a 2-D plane (low-speed streaks in red, where  $u \leq -0.3$ ), the black box marks the ramp region for Case I

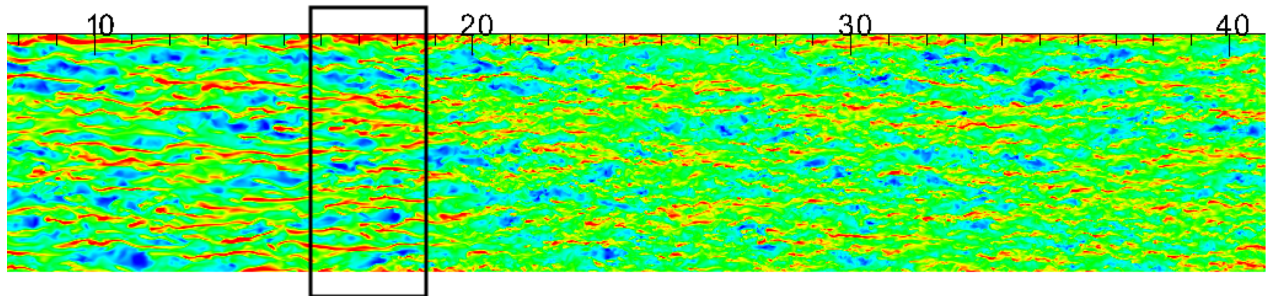


Fig. 11: Contour plots of  $u$  in a 2-D plane (low-speed streaks in red, where  $u \leq -0.3$ ), the black box marks the ramp region for Case II

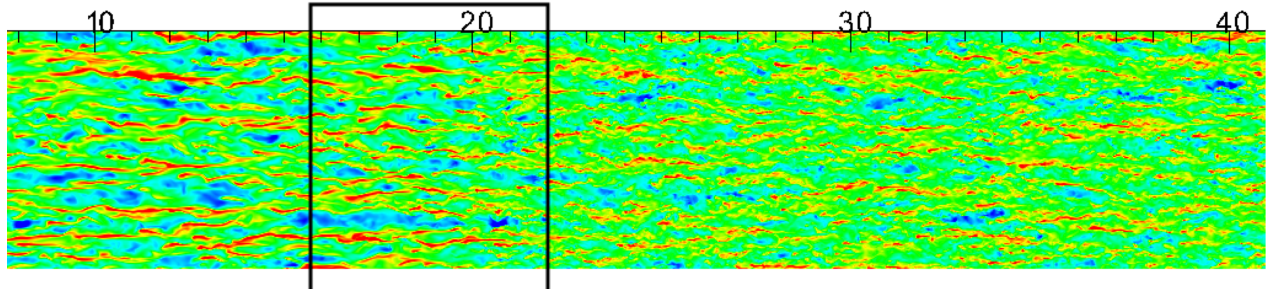


Fig. 12: Contour plots of  $u$  in a 2-D plane (low-speed streaks in red, where  $u \leq -0.3$ ), the black box marks the ramp region for Case III

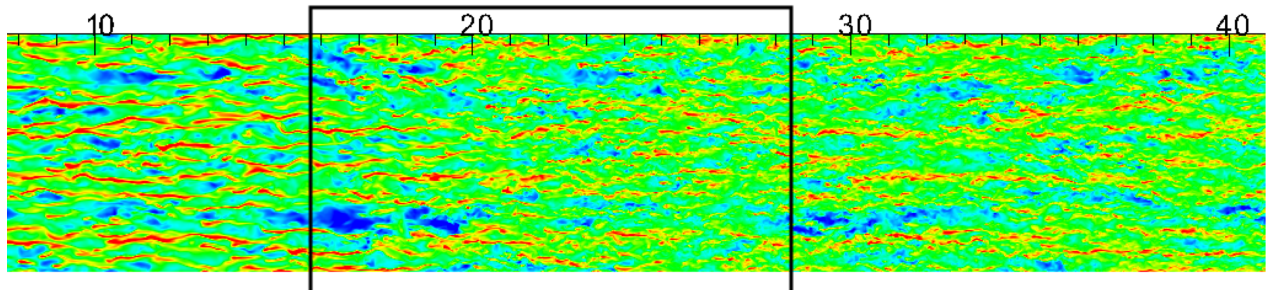


Fig. 13: Contour plots of  $u$  in a 2-D plane (low-speed streaks in red, where  $u \leq -0.3$ ), the black box marks the ramp region for Case IV

appears in the plots from Fig. 14 are actually the same as those reported in Tab. 2 for maximum values of  $Re_\tau$ .

In order to provide quantitative information on the low speed streaks, Fig. 15 presents the two-point  $R_{11}(\Delta z) = \langle u'(\mathbf{x})u'(\mathbf{x} + \Delta z) \rangle / R_{11}(\mathbf{x})$  correlation in the spanwise direction for the streamwise velocity fluctuations at  $y^+ = 5$ . In these plots, the greater is the value of the correlation  $R_{11}$ , the stronger will be the correlation between two distinct points separate by  $\Delta z$  in the spanwise direction. Thus, a good estimation of a coherent structure's size existing in the velocity field is provided when the correlation becomes zero. For Fig. 15, this value should be a good estimation of the streaks width  $W$ .

We observe that in Case I, Fig. 15a, the width of these structures does not change significantly, with value of  $W \approx 0.1$ , within the entire ramp region. It then suddenly decreases to  $W \approx 0.07$  at  $x_{peak} = 6.3\pi$ , i.e. roughly where the energy burst occurs. After that, the streaks' width remains

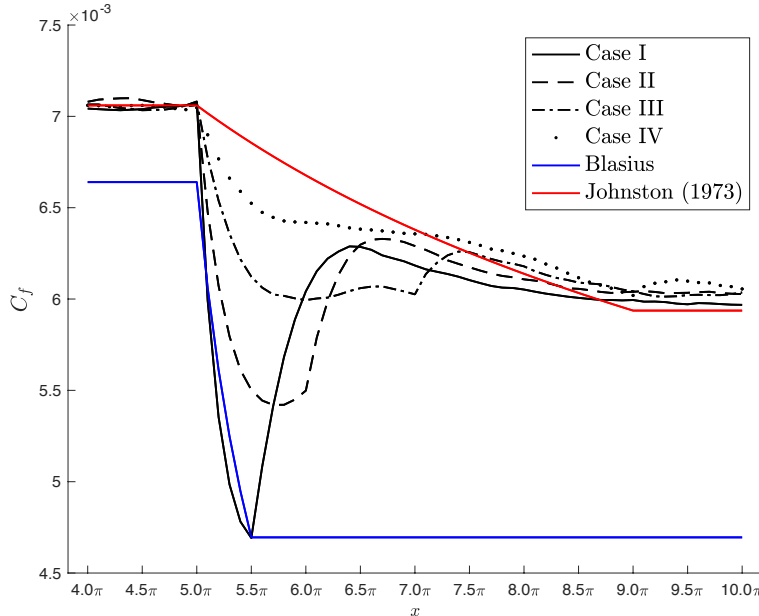
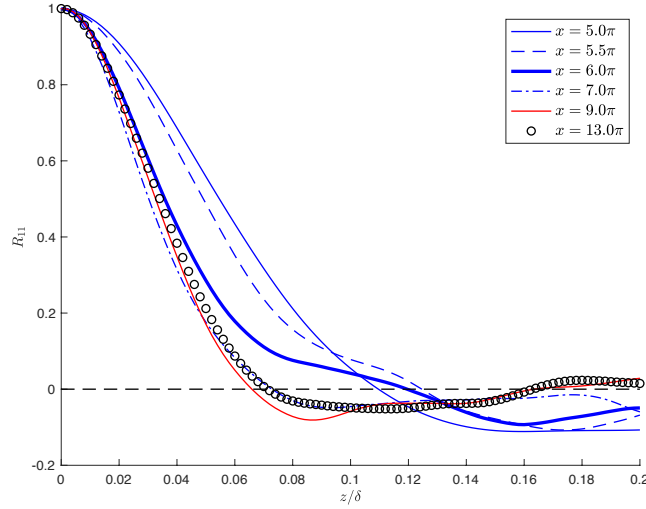


Fig. 14: The friction coefficient throughout the streamwise direction

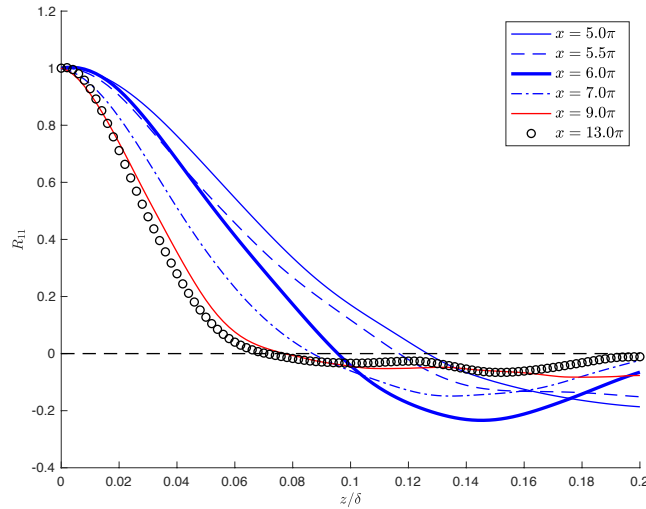
roughly unchanged through Region III. In contrast, the streaks in Case IV appear to evolve differently once they decrease in width along the ramp region. In this case,  $W$  decreases to the same ultimate size as in Case I, i.e.  $W \approx 0.7$ , however this time this size is reached already at the end of the ramp, at  $x = 9.0\pi$  and not in Region III. This way, we can infer from this scenario that the energy burst from Case I may be caused by the late breakdown of the streaks, which is delayed in space by the shorter ramp.

Additionally, Carlier and Stanislas in Ref. [30] found that the width of the streaks is between 20 and 40 wall units. This fact confers more reliability to our observations once the value of  $W \approx 0.1$  for streaks coming from Region I is equivalent to  $W^+ = 30$  in wall units, whereas the width  $W \approx 0.07$  belonging to Region III is equivalent to  $W^+ = 38$  in wall units, meaning that these sizes are in good agreement with Ref. [30].

Although various similarities are shared with the transient channel experiments, the root cause of the delays in these two scenarios are different. Ref. [4] explains that after a rapid flow rate excursion a thin boundary layer is formed in the near wall region which then progressively expands towards the core. The pre-existing turbulent structures act as initial perturbations to this new flow



(a) Correlation for Case 1.



(b) Correlation for Case 4.

Fig. 15: Two-point correlation in the spanwise direction of the streamwise velocity fluctuation for: (a) Case I and (b) Case IV

much like the role that the free-stream turbulence in a boundary bypass transition. The turbulent structures from the initial flow are modulated into elongated streaks which remain stable for a while, featuring the so called pre-transitional period. Later, in a stage referred as transitional phase, these elongated streaks become unstable and start breaking down into localized turbulent spots. With time, these turbulent spots grow in both streamwise and in spanwise directions and

eventually they occupy the entire wall surface marking the instant when the transition stages end and the flow becomes turbulent.

The transient channel setup imposes the conditions to change in the entire domain at once. Rather than that, the case considered in the present study imposes the flow's regime to change spatially. Obviously, the ramp's length  $R_{ramp}$  represents a major reason to cause the delay in the turbulence field as this parameter controls the fluid acceleration and the formation of a new boundary layer. By one side, a sharper ramp enhances these effects, by another side it also represents a ramp with a smaller length, which restricts these events in space. Under these conditions there is no physical way for the streaks coming from the first region to be modeled into stretched structures once the new boundary layer formed may interact with already existing structures after the ramp region. Instead, the low-speed streaks appear to keep their former characteristics and their streamwise length will determine the position in which these structures will start breaking down after Region II begins. In Ref. [30] it is confirmed that the streamwise size of streaks is typically between 500 and 2000 wall units, in that case the upper length in absolute values for these structures in Region I where  $Re_\tau = 300$  is roughly  $2\pi$ . This is a possible explanation why the  $Re_\tau$  obtained from the DNS from Fig. 6 is in agreement with the value corresponding to a fully developed right at  $x = 7\pi$  for Cases III and IV, i.e. after  $2\pi$  from the start of Region II.

## CONCLUSIONS

The present study marks the first investigation in turbulent flows undertaking a spatial ramp of imposed viscosity variations. In order to characterize flows undertaking this condition we have extended a turbulent channel in the streamwise direction, where the Reynolds number is imposed to linearly increase within a ramp region by means of changing the viscosity. Although a simplification, this set up well suits for the attempt to improve our understand of turbulence for flows subjected to spatially dependent properties, here the viscosity is considered. In this context, DNS are performed using Nek5000, a spectral-element code with large computational scaling capabilities. The models are developed such that three regions are considered: Region I, where viscosity remains constant and the flow is at  $Re = 5,000$ ; Region II, features a linear

ramp for the Reynolds with length  $L_{ramp}$  and; Region III, where the Reynolds remains constant again, now at  $Re = 10,000$ . Finally, four DNS varying the length of Region II were tested, namely  $L_{ramp} = 0.5\pi, 1\pi, 2\pi$  and  $4\pi$  were considered.

We observed different effects as response of the turbulence field due to the ramp imposed. Above all, friction does not respond immediately to the Reynolds number increase. As part of this investigation we developed a convolution function that served as a tool to model the spatial delay observed in the friction Reynolds number obtained from the DNS of the test cases. This analysis was useful to confirm how turbulence evolves progressively in Regions II and III. In the former, a delay is observed and appears to be the same regardless the ramp inclination imposed, also it appears to always terminate after a given length. In the last, turbulence bursts are observed as bumps are formed right at the beginning of Region III, moreover, these responses are severer as the ramp length is shortened.

In order to better characterize these effects, we have investigated the turbulence structures in the near wall region and turbulence statistics are collected for the computation of the TKE budget terms. Regarding the TKE budget terms for  $\langle u'u' \rangle$  component, we observe that the maximum production location shifts towards the core during the entrance of Region II in Cases I-III. This shift features a deviation from the well-known position for this maximum from  $y^+ \approx 11$  [27] moving up to  $y^+ \approx 14, 13$  and  $12$  in Cases I-III respectively. For Case IV on the other hand, this peak largely remains unchanged at  $y^+ \approx 11$ . Additionally, the only budget term that does not feature this shift in the vertical direction accordingly to the production is the viscous diffusion.

Furthermore, after the ramp region the budget terms clearly overshoots the ultimate energy distribution for Region III in Cases I-III. Rather than progressively evolving in a final energy distribution, these three cases features an energy burst at the beginning of Region III reaching a maximum at  $x_{peak}$  and only after that the energy profiles gets redistributed and converges into a final profile. In this context, we provide a potential explanation for the energy burst based on the behavior of turbulent structures coming from Region I.

The low-speed streaks in the viscous layer appears to play an important role that may explain the effects taking place in the turbulence field. To understand that, we observe that the viscous

forces decreases in the ramp, for this reason an attenuation in turbulence is expected similarly to the test cases from Refs. [11–14]. This becomes particularly evident through Fig. 14 where we compare the skin friction coefficient  $C_f$  of the four test cases with the values yielded by the Blasius solution within a  $L_{ramp} = 0.5\pi$  ramp, and the values yielded by the Johnston’s correlation [29] valid for fully developed turbulent flow. From this plot we observe that not only the DNS  $C_f$  is lower than the Johnston’s correlation for all cases, but also a good agreement is found between the DNS result and the Blasius solution for Case I, meaning that in general turbulence is attenuated due to the ramp and in fact the flow behaves laminar-like for the shortest ramp tested.

We explain this in terms of the dynamic of turbulent structures. Streaks coming from Region I start breaking down due a reduction in viscous forces I, but such breakdown is delayed in space due to spatial development. The size of the delay is related to the streamwise size of the streaks. For short ramps (e.g., Case I), this process only occurs at the beginning of Region III, where the energy burst is observed. We confirmed this in a quantitative fashion, by estimating the width of the streaks at different streamwise positions through two-point correlation of the streamwise velocity in the spanwise direction (Fig 15). On the other hand, for softer ramps the width of the streaks in decrease progressively along the ramp region, reaching its minimum and steady value at the end of the ramp. However, the delay in first part of the ramp remains the same for all cases.

## REFERENCES

- [1] Coppo Leite, V., and Merzari, E., 2020. “The effect of varying viscosity in turbulent channel flow”. Vol. 3: Computational Fluid Dynamics; Micro and Nano Fluid Dynamics of *Fluids Engineering Division Summer Meeting*. V003T05A019.
- [2] Zonta, F., Marchioli, C., and Soldati, A., 2012. “Modulation of turbulence in forced convection by temperature-dependent viscosity”. *Journal of Fluid Mechanics*, **697**, p. 150–174.
- [3] Zonta, F., Onorato, M., and Soldati, A., 2012. “Turbulence and internal waves in stably-stratified channel flow with temperature-dependent fluid properties”. *Journal of Fluid Mechanics*, **697**, p. 175–203.
- [4] He, S., and Seddighi, M., 2013. “Turbulence in transient channel flow”. *Journal of Fluid*

- Mechanics*, **715**, p. 60–102.
- [5] Andersson, P., Berggren, M., and Henningson, D. S., 1999. “Optimal disturbances and bypass transition in boundary layers”. *Physics of Fluids*, **11**(1), pp. 134–150.
  - [6] Brandt, L., and Henningson, D. S., 2002. “Transition of streamwise streaks in zero-pressure-gradient boundary layers”. *Journal of Fluid Mechanics*, **472**, p. 229–261.
  - [7] Maruyama, T., K. T., and Mizushima, T., 1976. “The structure of the turbulence in transient pipe flows”. *Journal of Chemical Engineering of Japan*, **9**(6), pp. 431–439.
  - [8] He, S., and Jackson, J. D., 2000. “A study of turbulence under conditions of transient flow in a pipe”. *Journal of Fluid Mechanics*, **408**, p. 1–38.
  - [9] Greenblatt, D., and Moss, E. A., 2004. “Rapid temporal acceleration of a turbulent pipe flow”. *Journal of Fluid Mechanics*, **514**, p. 65–75.
  - [10] He, S., and Seddighi, M., 2015. “Transition of transient channel flow after a change in reynolds number”. *Journal of Fluid Mechanics*, **764**, p. 395–427.
  - [11] Kline, S. J., Reynolds, W. C., Schraub, F. A., and Runstadler, P. W., 1967. “The structure of turbulent boundary layers”. *Journal of Fluid Mechanics*, **30**(4), p. 741–773.
  - [12] Patel, V. C., and Head, M. R., 1968. “Reversion of turbulent to laminar flow”. *Journal of Fluid Mechanics*, **34**(2), p. 371–392.
  - [13] Narayanan, M. A. B., and Ramjee, V., 1969. “On the criteria for reverse transition in a two-dimensional boundary layer flow”. *Journal of Fluid Mechanics*, **35**(2), p. 225–241.
  - [14] Blackwelder, R. F., and Kovasznay, L. S. G., 1972. “Large-scale motion of a turbulent boundary layer during relaminarization”. *Journal of Fluid Mechanics*, **53**(1), p. 61–83.
  - [15] Webster, D. R., Degraaff, D. B., and Eaton, J. K., 1996. “Turbulence characteristics of a boundary layer over a two-dimensional bump”. *Journal of Fluid Mechanics*, **320**, p. 53–69.
  - [16] Muck, K. C., Hoffmann, P. H., and Bradshaw, P., 1985. “The effect of convex surface curvature on turbulent boundary layers”. *Journal of Fluid Mechanics*, **161**, p. 347–369.
  - [17] Baskaran, V., Smits, A. J., and Joubert, P. N., 1987. “A turbulent flow over a curved hill part 1. growth of an internal boundary layer”. *Journal of Fluid Mechanics*, **182**, p. 47–83.
  - [18] Fischer, P. F., 1997. “An overlapping schwarz method for spectral element solution of the

- incompressible navier–stokes equations”. *Journal of Computational Physics*, **133**(1), pp. 84–101.
- [19] Fischer, P., Lottes, J., Kerkemeier, S., Marin, O., Heisey, K., Obabko, A., Merzari, E., and Peet, Y., 2015. Nek5000: Users manual. Tech. rep.
- [20] Patera, A. T., 1984. “A spectral element method for fluid dynamics: Laminar flow in a channel expansion”. *Journal of Computational Physics*, **54**(3), pp. 468 – 488.
- [21] Merzari, E., Pointer, W., and Fischer, P., 2013. “Numerical simulation and proper orthogonal decomposition of the flow in a counter-flow t-junction”. *Journal of Fluids Engineering*, **135**, 09, p. 091304.
- [22] Dillon, S., Obabko, A., Tomboulides, A., Coppo Leite, V., Lan, Y. H., Min, M., Fischer, P., and Boyd, C., 2020. Nek5000 developments in support of industry and the NRC. Tech. rep.
- [23] Lee, M., and Moser, R. D., 2015. “Direct numerical simulation of turbulent channel flow up to  $Re_\tau \approx 5200$ ”. *Journal of Fluid Mechanics*, **774**, p. 395–415.
- [24] Pope, S. B., 2000. *Turbulent Flows*. Cambridge University Press, New York.
- [25] Oppenheim, A. V. Signals and systems. On MIT OpenCourseWare. URL <http://ocw.mit.edu>.
- [26] Kaoru Iwamoto, Y Suzuki, N. K., 2002. Database of fully developed channel flow. Tech. rep.
- [27] Fernholz, H., and Finleyt, P., 1996. “The incompressible zero-pressure-gradient turbulent boundary layer: An assessment of the data”. *Progress in Aerospace Sciences*, **32**(4), pp. 245 – 311.
- [28] Schlichting, H., and Gersten, K., 2017. *Boundary-Layer Theory*. 01.
- [29] Johnston, J. P., 1973. “The Suppression of Shear Layer Turbulence in Rotating Systems”. *Journal of Fluids Engineering*, **95**(2), 06, pp. 229–235.
- [30] Carlier, J., and Stanislas, M., 2005. “Experimental study of eddy structures in a turbulent boundary layer using particle image velocimetry”. *Journal of Fluid Mechanics*, **535**, p. 143–188.